

Phase Reconstruction of a Cu(001) Seed Layer from *in situ* Polarized Neutron Reflectometry Data using Fe Reference Layers

Alexander Book^a, Sina Mayr^{a,1}, Jochen Stahn^b, Peter Böni^a, Wolfgang Kreuzpaintner^{a,c,d}

^aTechnische Universität München, Physik-Department E21, James-Franck-Str. 1, 85748 Garching, Germany

^bLaboratory for Neutron Scattering and Imaging, Paul Scherrer Institut, 5232 Villigen PSI, Switzerland

^cInstitute of High Energy Physics, Chinese Academy of Sciences (CAS), Beijing 100049, China

^dSpallation Neutron Source Science Center (SNSSC), Dongguan 523803, China

Abstract

The reconstruction of the complex reflection coefficient obtained by *in situ* Polarized Neutron Reflectometry is presented. Using the reference layer method, with a magnetic Fe layer, the phase information of the underlying Cu(001) seed layer sample structure is successfully retrieved and its scattering length density is calculated and compared with results obtained from traditional fitting. Two different reference layer approaches for retrieving the phase information are compared.

Keywords: Neutron Reflectometry, Thin Film, Phase Reconstruction, Reference Layer, Phase Problem

1. Introduction

Polarized Neutron Reflectometry (PNR) is an indispensable scattering technique to probe structural and magnetic properties of thin films and heterostructures. The desired physical parameters are commonly extracted by fitting an appropriate theoretical model to the measured reflectivity. However, without any *a-priori* knowledge of the sample structure, a manifold of scattering potentials can yield the same reflectivity since the phase information is not preserved in the measurement. This ambiguity is known as the phase problem.

Various solutions to the phase problem in neutron and x-ray reflectometry have been proposed: Fiedeldey et al. [1] use an ordinary differential equation involving the dwell time (viz. the time the neutron “stays” inside the sample) to solve for the reflection phase. Clinton [2] uses a logarithmic dispersion relation to associate the phase with the reflectivity in the Born-Approximation. Experimentally oriented solutions usually vary known segments of the sample to constrain the phase.

Another idea consists of utilizing specific materials which exhibit resonance effects for wavelengths close to absorption edges, mainly for x-rays [3]. These materials serve as references which vary their SLD depending on the wavelength while the SLD of the unknown part of the sample is constant. For neutron reflectometry in the thermal to epithermal range, rare earths are suitable candidates

as absorbing materials [4] and corresponding experiments have been performed [5, 6, 7].

In the reference layer method [8, 9] one varies the scattering length density (SLD) by changing the magnetization of the sample [10], by using buried or fronting layers of different SLDs [11, 12] or by a variation of sample’s surroundings [13]. Other approaches use an adapted version of the reference layer method by measuring the polarization of the reflected neutrons instead of the reflectivity for assessing the phase below the critical edge [14, 15].

To uniquely determine the scattering potential for *in situ* PNR, we reconstructed the phase information of a model system, i.e. a Cu seed layer, by applying the fronting reference layer method [16]. We successively increased the thickness of the top Fe reference layer and after each Fe deposition step we inspected the sample by *in situ* PNR. The usage of Fe as a fronting material allows us to increase the contrast by magnetizing the reference layer, thus improving the quality of the phase information. We present two reference layer approaches, viz. the remnant Fe layer approach in Section 4.1 and an improvement by incorporating the remnant Fe layer into the reference in Section 4.2. Finally, we extrapolated the reflection to further assess the results from the inverted SLD.

This work demonstrates a proof of concept of the application of a phase reconstruction technique for *in situ* PNR. It is shown that *in situ* PNR is well suited for phase reconstruction since a large number of reference layers can be created and measured with the very same underlying sample.

Email address: alexander.book@frm2.tum.de (Alexander Book)

¹Present address: Paul Scherrer Institut, 5232 Villigen PSI, Switzerland

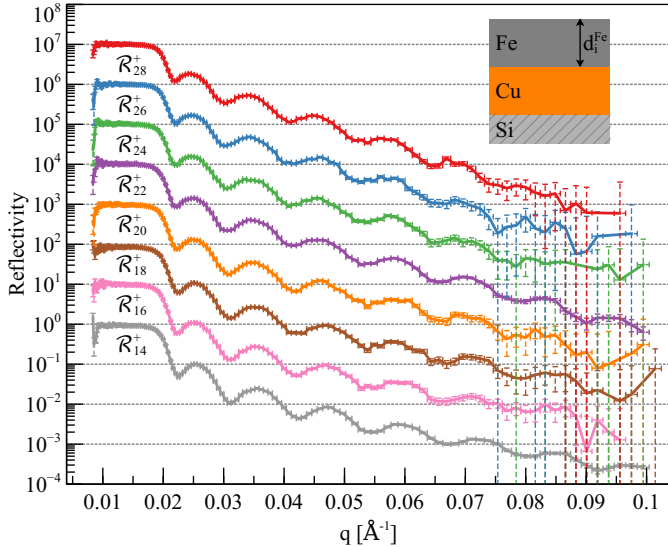


Figure 1: Reflectivity data of the Si/Cu/Fe sample with varying Fe layer thickness. Each reflectivity is shifted by one order of magnitude for clarity. The reflectivity curve \mathcal{R}_n^+ corresponds to the sample with n monolayers of Fe on top with the Fe layer being magnetized parallel to the neutron spin polarization. The inset depicts the sample's layer structure.

2. Experimental Procedure

A 45 nm thick Cu seed layer was grown on a $2\text{ cm} \times 2\text{ cm}$ Si(001) substrate using DC magnetron sputtering in an ultrahigh-vacuum deposition chamber [17, 18]. Subsequently, a 7 nm thick Fe thin film was added on the Cu layer in 28 deposition steps with a growth rate of approximately one monolayer of Fe per deposition step. PNR measurements are carried out after each deposition step; after the 14th deposition, only every second step is monitored by PNR [19]. The deposition and PNR measurements were performed on the neutron reflectometer Amor at the Swiss Spallation Neutron Source (SINQ), Paul Scherrer Institut, Villigen [20]. The resulting spin-up (+) and spin-down (-) reflectivity is denoted by \mathcal{R}_i^\pm . Figure 1 depicts the performed PNR measurements for the deposition steps 14 to 28 which will be used for reconstructing the reflection of the Cu seed layer. The reflectivity \mathcal{R}_{14} is shown for completeness.

To reconstruct the Cu seed layer, we employ the reference layer method described in [16] by using the top Fe layer as the reference. In the process of reconstruction, the contribution of the Fe layer on the reflection will be eliminated and only the reflection of Si/Cu will be retrieved. For the reconstruction we use seven different sample configurations, yielding in total 14 PNR measurements.

It is noted that the requirements [21, 16] of the SLD for the reconstruction are all fulfilled, namely: All the constituents of the sample (Si, Cu, Fe) have a SLD with non-negative real part (hence no bound states [21]) and the imaginary part is sufficiently small (≈ 4 orders of magnitude smaller compared to the real part) which justifies the assumption that the SLD is completely real valued. The

sample is also of finite extent regarding its top surface and we assume that the unknown portion of the sample (i.e. Si/Cu) remains constant in each Fe deposition step.

3. Data Analysis

The reflection R is the complex amplitude of the wave function of the neutrons $\psi(z) \sim 1e^{-iqz} + Re^{iqz}$ as $z \rightarrow \infty$, hence the neutrons are impinging on the scattering potential from the right in Figure 2. The reflectivity $|R|^2$ is the squared modulus of the reflection R and the phase $\phi = \arg(R)$ is correlated with the reflection by $R = |R|e^{i\phi}$.

In general it is sufficient to use three PNR measurements of the same sample with different reference layers to unambiguously reconstruct the reflection R from inversion of a 3×3 “constraint”-matrix and to obtain a reflection parameter vector $\Theta = (\alpha, \beta, \gamma) \in \mathbb{R}^3$. Here, α, β and γ originate from the elements of the transfer-matrix [8]. In the matrix formulation of the one dimensional Schrödinger equation the transfer-matrix relates the reflected to the transmitted plane wave within a thin film. The reflection R is calculated from the reflection parameter vector Θ by

$$R = \frac{\beta - \alpha - 2i\gamma}{\alpha + \beta + 2}. \quad (1)$$

We can incorporate $N \in \mathbb{N}$ measurements by using a chi-squared (χ^2) ansatz

$$\chi^2(\Theta) = \sum_{i=1}^N \left(\frac{L_i \cdot \Theta - b(|R_i|^2)}{\sigma_{b(|R_i|^2)}} \right)^2, \quad (2)$$

and solve for the χ^2 -minimizing reflection parameter Θ . The minimizer of χ^2 can be analytically computed by the linear least squares method. The solution exists and is unique since there are more measurements than unknowns and the least squares matrix $L = (L_i)_i^N$ has full rank. In this ansatz, the vector $L_i \in \mathbb{R}^3$ contains the reference layer information (i.e. the complete SLD profile of the reference layer) and $b(|R_i|^2)$ is a transformed reflectivity measurement with standard deviation $\sigma_{b(|R_i|^2)}$:

$$b(|R_i|^2) \sim \frac{1 + |R_i|^2}{1 - |R_i|^2} \quad (3)$$

This shows why the reconstruction can only work outside the total reflection regime, since the denominator $1 - |R_i|^2 = 0$ for total reflection.

With the usage of the χ^2 ansatz, the uncertainty in the reflectivity data can be taken into account and the resulting reflection can be reconstructed more precisely, due to better statistics of the multiple reflectivity data sets and due to the reduction of the error in the SLD profile of the reference layer. In particular the last point is worth noting: It is highly complicated to precisely determine the shape of the reference layers which are required for the reconstruction. However, by incorporating multiple measurements, the importance of a precise knowledge of the

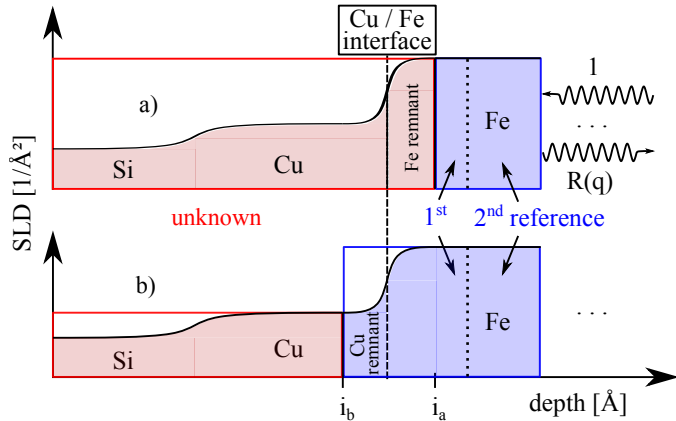


Figure 2: Schematic comparison of two different reference layer selections. The blue shaded area on the right depicts the reference layer whereas the left area is the unknown sample. a) The remnant Fe layer is shifted to the unknown part of the sample. b) The full Fe layer, containing interdiffusion and/or roughness of the Cu/Fe interface, is included into the reference.

reference layer appears to decrease. This is a key property from which we take advantage in this paper.

The reflection is inverted using the Gelfand-Levitan-Marchenko (GLM) method [22] to retrieve the SLD. We use only the real part of the reflection, as applying the imaginary part resulted in singularities that cannot be resolved. It is noted that we can freely choose either one of the real or imaginary quantities, as they yield the same SLD [21]. The software used for the reconstruction and potential inversion is available freely [23, 24].

4. Results

The sample is virtually split into two parts at a depth i ; an unknown part and a reference layer. The splitting point i can be chosen arbitrarily, but only a few specific ones are physically meaningful (see Figure 2). The variables i_a and i_b denote the depths inside the sample at which the SLD is completely characterized by only one of the contributions of Fe or Cu, respectively:

Splitting the sample at $i = i_a$ assigns the remnant Fe layer to the unknown sample. This case is investigated in Section 4.1. The advantage of this approach is that it does not require knowledge of the Cu/Fe interface, however, due to the magnetism in the Fe layer, only data of one spin direction can be used. Alternatively, the splitting at $i = i_b$ allows both spin direction data to be used, since the unknown sample is non-magnetic, but this requires additional *a-priori* knowledge of the Cu/Fe interface.

In the following it is shown that using only measurements of one spin direction (Section 4.1) is sufficient to reconstruct the reflection. However, significant improvements in the quality of the reconstruction can be obtained by using the experimental data of both spin directions (Section 4.2).

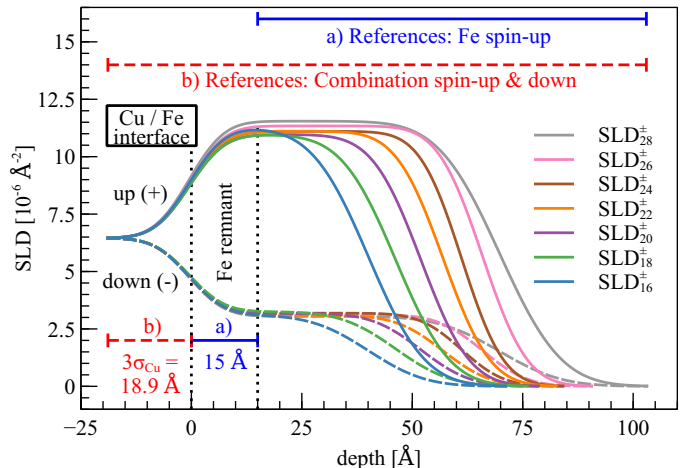


Figure 3: The SLD profiles of the reference layers, scaled such that a depth of 0 Å refers to the Cu/Fe interface. a) Spin-up SLDs of reference layers with a remnant Fe layer (Section 4.1). b) Reference layers comprising the full Fe layer and including the Cu/Fe interface for both spin channels (Section 4.2).

Table 1: Fitted parameters of the Fe reference layer and of the unknown layer (from [19]).

Name	thickness d [Å]	density ρ [g/cm ³]	roughness σ [Å]	magnetization M [μ_B /atom]
\mathcal{R}_{28}	70.3	7.16	11.0	2.03
\mathcal{R}_{26}	66.4	7.09	8.0	1.98
\mathcal{R}_{24}	61.7	7.01	7.5	1.93
\mathcal{R}_{22}	57.5	6.96	8.4	1.97
\mathcal{R}_{20}	52.5	6.94	8.7	1.92
\mathcal{R}_{18}	46.8	6.97	9.7	1.89
\mathcal{R}_{16}	40.6	7.05	10.1	1.98
\mathcal{R}_{14}	36.7	6.95	9.3	1.91

	d [Å]	ρ [g/cm ³]	σ [Å]	SLD [Å ⁻²]
Cu	451	8.82	6.3	6.45×10^{-6}
Si	∞	2.33	10.7	2.08×10^{-6}

It is noted that by specular reflectivity alone roughness and interdiffusion cannot be distinguished; henceforth the term roughness also includes interdiffusion and vice versa.

4.1. Reconstruction Using a Remnant Fe Layer

The top Fe layer represents the reference, however the Fe layer thickness is constrained and a part of it (remnant Fe) is declared to belong to the unknown part (Figure 2a). It is noted that the remnant layer has a non-zero magnetization which prohibits the use of both spin state reflectivity measurements for reconstructing the reflection.

Figure 3 depicts the SLD profile of the reference layers. Each reflectivity measurement \mathcal{R}_i^\pm has a corresponding reference layer SLD $_i^\pm$ which is used for the reconstruction of the reflection. *In situ* thin film growth allows the thickness of the deposited Fe layer to be known *a-priori*, however, the parameters used for describing the SLD of the Fe

reference layer were extracted using a traditional fitting method [19]. These are listed in Table 1 for $\mathcal{R}_{14} - \mathcal{R}_{28}$.

Here, we use the reference layers configuration shown in Figure 3a. The roughness at the Cu/Fe interface is assumed to be smaller than $3\sigma = 15 \text{ \AA}$. This restricts the usable reflectivity measurements to those in the deposition steps 6 to 28, viz. $\mathcal{R}_6 - \mathcal{R}_{28}$. To further simplify the shape of the reference layers only those with a thickness significant above $\approx 35 \text{ \AA}$ are considered, viz. $\mathcal{R}_{16} - \mathcal{R}_{28}$. We selected the spin-up reflectivity \mathcal{R}^+ since it has better statistics for higher q wave vector transfers. The case of using only spin-down reflectivities is given in Appendix A.

Figure 4a shows the reconstructed reflection. It exhibits low frequency oscillations from the Cu layer and high frequency oscillations, which result from the measurement noise in the reflectivity (for more details see Appendix A). The expected reflection is the theoretically calculated reflection based on fitted parameters given in Table 1.

The reflection below the critical edge $q_c = \sqrt{16\pi\text{SLD}}$ was retrieved using the fixed-point algorithm described in [25]. Note that this particular algorithm only guarantees a successful retrieval if the product of film thickness and minimal wave vector transfer is smaller than 2π . This is, however, not given in our case, as the Cu layer is thicker than 400 \AA and the minimal wave vector is $\approx 0.023 \text{ \AA}^{-1}$. To ensure the algorithm to converge, a 150 \AA thick portion of the unknown Cu layer was assigned to the SLD of bulk Cu ($\text{SLD}_{\text{Cu}} = 6.554 \times 10^{-6} \text{ \AA}^{-2}$ [26]). It was positioned inside the Cu layer between $200 \text{ \AA} \leq \text{depth} \leq 350 \text{ \AA}$. Variations of the position ($\pm 50 \text{ \AA}$) or thickness ($150 \text{ \AA} - 250 \text{ \AA}$) of the bulk Cu portion did not substantially change the retrieved reflection.

The corresponding inverted SLD is displayed in Figure 4b and the dotted curve shows the slab model which is used for calculating the expected reflection. At the Si/Cu interface (between a depth of -20 \AA and 20 \AA) the inverted SLD matches the expected SLD remarkably well. However, the inverted SLD in general exceeds the expectation, except at the dip at the center $\approx 200 \text{ \AA}$ or at the remnant Fe layer $\approx 450 \text{ \AA}$. The quality of the reconstructed reflection is not sufficient to draw other conclusions beside estimating the Cu layer thickness.

4.2. Reconstruction by Combination of Spin-Up and Down Measurements

To improve the quality of the reconstructed reflection, spin-down and spin-up measurements are used together. To increase the contrast and to allow for this approach, the remnant Fe layer needs to be part of the reference instead of the unknown sample. Only this allows the unknown part of the sample to be non-magnetic. Therefore, knowledge of the interface roughness of the Cu layer and density at the interface is needed, since these parameters determine the shape of the reference at the Cu/Fe interface. We use the fitted values for the interface (Table 1), however, it is noted that no substantial change in

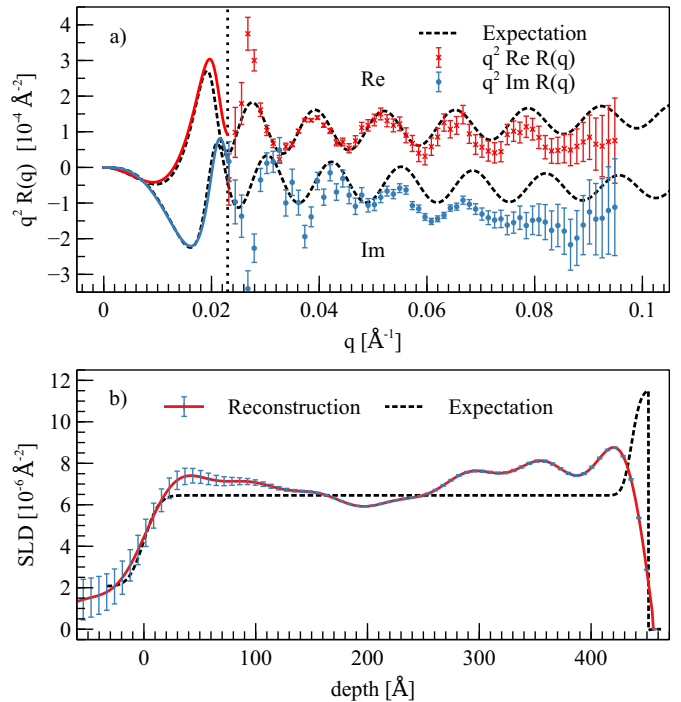


Figure 4: a) Reconstructed reflection multiplied with q^2 of the unknown Cu layer, including a remnant Fe layer (see figures 2a and 3a). The reflectivity data $\mathcal{R}_{16}^+ - \mathcal{R}_{28}^+$ is used for the reconstruction. The expected curve (dashed line) represents the reflection of the fitted model which is a 436 \AA thick Cu layer on a Si substrate with a 15 \AA thick magnetized Fe layer on top. The reflection below the critical edge $q \leq 0.023 \text{ \AA}^{-1}$ (dotted vertical line) is numerically retrieved and its error is set to zero. b) Inverted SLD using the real part of the reflection in (a).

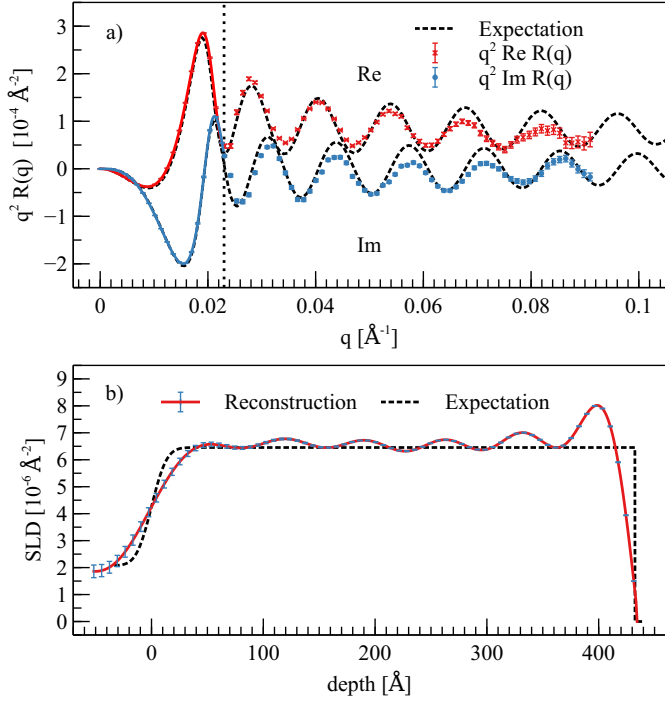


Figure 5: a) Reconstructed reflection multiplied with q^2 of the unknown Cu layer (see figures 2b and 3b), using the reflectivity data $\mathcal{R}_{16}^{\pm} - \mathcal{R}_{28}^{\pm}$. The dashed curves represent the expected reflection of the fitted model. The reflection for $q \leq 0.023 \text{ \AA}^{-1}$ (dotted line) is numerically retrieved. b) Inverted SLD using the reflection shown in (a). The dotted line represents the potential retrieved via classical fitting.

the reflection was observed if only approximate parameters ($\text{SLD}_{\text{Cu}} = 6.554 \times 10^{-6} \text{ \AA}^{-2}$, $\sigma_{\text{Cu/Fe}} = 5 \text{ \AA}$) are used instead. The reference layer SLDs as used in the following are shown in Figure 3b.

The reconstructed reflection is given in Figure 5a. The missing reflection $R(q)$ for $q \in [0, 0.023] \text{ \AA}^{-1}$ is retrieved by the fixed-point algorithm as described in Section 4.1. Figure 5b shows the resulting inverted SLD. By using both spin direction measurements, the reconstructed SLD more closely resembles the fitted SLD, if compared to previous results (Figure 4b)), and the pronounced dip in the center of the potential at a depth of 200 \AA is reduced.

4.3. Fitting the Reflection

To eliminate the remaining oscillations in the inverted SLD, knowledge of the reflection for a larger q range is required [27]. The truncation of the reflection is currently one of the reasons why an even more precise potential inversion is not yet possible. Here, we demonstrate how an extrapolation of the given data allows the oscillations in the resulting potential to be eliminated: We fit a model function to the reflection data multiplied with q^2 and extrapolate the fitted model parameters to $q = 5 \text{ \AA}^{-1}$. As a

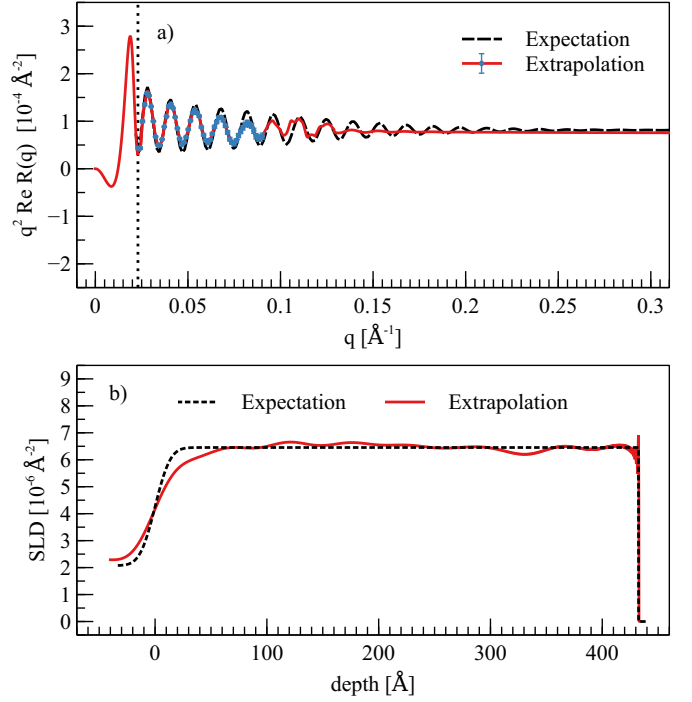


Figure 6: a) Extrapolated real part of the reflection multiplied with q^2 (solid curve) using model (4). The reflection below $q = 0.023 \text{ \AA}^{-1}$ (dotted line) is numerically retrieved and above $q = 0.085 \text{ \AA}^{-1}$ is extrapolated. The blue dots correspond to the reconstructed reflection from measurement data. b) Inverted SLD using the extrapolated reflection (see (a)) $R(q)$ for $0 \text{ \AA}^{-1} \leq q \leq 5 \text{ \AA}^{-1}$.

model function for the real part of the reflection we use

$$\begin{aligned}
 q^2 \text{Re } R(q) &= O(q) - A(q) \cos(qd + \phi_0 + \phi_1 q^{-1}), \\
 O(q) &= 4\pi\rho + a_1 q^{-1}, \\
 A(q) &= \left(4\pi\rho_{\Delta} + \frac{a_0}{q - q_c}\right) e^{-q^2 \sigma^2}.
 \end{aligned} \tag{4}$$

The amplitude $A(q)$ and offset $O(q)$ function are selected heuristically such that they agree with a single layer model in the Born-Approximation when taking the limit $q \rightarrow \infty$. The parameter σ is the roughness or interdiffusion of the Cu/Si interface, d determines the Cu layer thickness, $\phi_1 q^{-1}$ is a first order correction term to take the non-linearity of the periodicity into consideration. The offset ρ is the SLD of Cu and ρ_{Δ} is the difference in the SLD of Cu and Si (see Table 1). The remaining parameters have no physical relevance. The best least-squares fitting parameters are listed in Table B.1 in Appendix B.

The extrapolated reflection is depicted in Figure 6a. A clear deviation from the expected reflection can be observed, especially in the limit $q \rightarrow \infty$. Nevertheless, inverting the extrapolated reflection yields the SLD shown in Figure 6b. The small and sharp peak at the Cu/Fe interface at a depth of $\approx 430 \text{ \AA}$ is due to the Gibbs-phenomena [28]

Table 2: Comparison of the layer parameters obtained by using different reference layers.

Method	Si		Cu	
	ρ [g/cm ³]	σ [Å]	ρ [g/cm ³]	d [Å]
Only spin-up	2.01	24.1	9.63	427
Spin-up & down	2.20	17.7	8.93	426
Extrapolation	2.57	12.3	8.83	432
Traditional fit	2.33	10.7	8.82	432 ^a

^a after subtracting $3\sigma_{\text{Cu/Fe}} \approx 19 \text{ \AA}$

5. Discussion

The reconstruction of an Fe remnant layer shows the possibility to use monolayers of Fe as a reference and to successfully retrieve the reflection. However, we observed high frequency oscillations over the entire q range under investigation (Figure 4a) if compared with the expected reflection. We suspect the Poisson noise in the reflectivity data to cause the oscillations in the reconstructed reflection. This assumption is supported by the observation of a similar behavior when only simulated data is used. Simulations comparing the effect of the resolution onto the reconstructed reflection (Appendix C) suggest that the resolution does not contribute to the high frequency oscillations, but that it only dampens the amplitude of the reflection.

The large errors at high q originate from the unsatisfactory signal-to-noise ratio of the reflectivity measurements when the reflectivity is of the same order of magnitude as the background. Applying the remnant layer approach to spin-down reflectivity measurements yields larger errors in the reflection (Figure A.2 in Appendix A) than applying it to the spin-up reflectivity data. Appendix A discusses the effect of noise in more detail. Nonetheless, the retrieved profile shows in general a good agreement with the expected slab model, except at the jump discontinuity (Figure 4b) at a depth of 400 Å - 450 Å.

Improvements of the reconstruction can be achieved by combining spin-up and down reflectivity measurements, although the parameters of the interface between the unknown part of the sample to the references have to be estimated, which is in principle an information that one wants to obtain from the experiment.

Nevertheless, the advantage of using the combined approach is the much higher contrast of the SLDs, which result from using magnetic materials and all the available PNR data. Hence, the reconstructed reflection has a strongly improved accuracy and agreement with the expected reflection, which yields a more accurate inverted SLD. It is noted that the errors in Figure 5b are calculated with estimated errors in the low q reflection regime (see Appendix D for details), whereas the errors in Figure 4b are neglected.

Table 2 compares the structural parameters of the Si

substrate and Cu layer retrieved by a phase reconstruction with the parameters obtained from traditional fitting. The Cu layer thicknesses are consistent with the fitted parameter as they differ by a mere $\approx 6 \text{ \AA}$. It is noted that the reference layer includes the Cu/Fe roughness/interdiffusion transition, which causes the reconstructed Cu layer to be $3\sigma_{\text{Cu/Fe}} \approx 19 \text{ \AA}$ thinner. The rms roughness at the Si/Cu interface substantially differs from the fitted roughness. The deviation can be explained by the fact that the fitting model allowed the resolution to be varied, whereas for reconstruction of the reflection the resolution is not taken into account, see Appendix C.

The densities of the Si substrate and the Cu layer are estimated by the average SLD. They agree with the fitted densities and are in line with the values reported in the literature. The noise inherent in the reflection which is reconstructed using only spin-up measurements is preventing a precise inversion of the SLD.

By extrapolating the reflection to higher q a smoothing of the oscillations in the SLD is observed and only small deviations $\leq 4\%$ to the expected model of the SLD inside the Cu layer are identified. To the right of the Si/Cu interface at a depth of 25 Å a mismatch of $\approx 13\%$ is visible due to the resolution of the reconstructed reflection. The deviation in the Si SLD of $\approx 10\%$ originates from the mismatch in ρ_{Δ} , which can be improved by utilizing a more sophisticated model for the reflection extrapolation.

6. Summary and Conclusion

We have shown the applicability of the reflection reconstruction with magnetic reference layers to retrieve the reflection of a seed layer for the case of *in situ* PNR. Only the top Fe layers are used as a reference layer. On the one hand, splitting the total Fe layer in a remnant and reference part allows the underlying unknown sample to be reconstructed without any further assumptions, but with a reduction of accuracy as only reflectivity measurements of the same spin direction can be used. On the other hand, if one assumes knowledge of the Cu/Fe interface it is possible to use all performed spin-up and spin-down PNR measurements to obtain a more precise reflection.

The parameters extracted of the unknown sample are in general consistent with the values obtained from traditional data fitting. Only the roughness parameters substantially differ from the fitted value which we attribute to the resolution degradation. Nevertheless, we have shown to uniquely extract the desired parameters like roughness, density and thickness of the unknown sample by means of phase-sensitive *in situ* PNR.

The presented analysis technique finds its application in the unique determination of depth resolved magnetism such as proximity effects like induced magnetism between heavy-metal and ferromagnetic transition metals (FM) [29, 30]. Additionally, it allows the morphology of thin film system with magnetic tunnel junctions in FM/oxide/FM

structures (e.g. Fe/MgO/Fe) [31, 32], or multilayer systems like Fe/Gd or Pt/Co/Ta, which are known to show a formation of skyrmions at room temperature [33, 34], to be precisely investigated. It is noted that, although we used ferromagnetic reference layers, the technique of *in situ* growth allows non-magnetic reference layers to be applied in order to probe an unknown magnetic part of a sample.

In light of the upgrade of the Selene focusing optics at Amor, PSI and the advent of the new beamline Estia at the European Spallation Source (ESS) a tremendous improvement in the acquired data quality is expected, which will entail a reduction of statistical noise and in turn facilitate even more precisely reconstructed reflections. The limitation of the q range in the reflection will be lessened, as the upgrade allows much higher q values to be assessed at a given data acquisition time, enabling more accurate sample descriptions to be determined. In addition, phase determination in time-resolved polarized neutron reflectometry by *in situ* or *in operando* techniques might become viable, as it is already demonstrated for X-ray radiation [35, 36].

7. Acknowledgments

This work is based on experiments performed at the Swiss spallation neutron source (SINQ), Paul Scherrer Institute, Villigen, Switzerland. The research is funded by the Deutsche Forschungsgemeinschaft (DFG, German Research Foundation) within the Transregional Collaborative Research Center ‘‘From electronic correlations to functionality’’ - Projekt ID 107745057 - TRR 80.

Appendix A. Influence of Poisson Noise on the Reflection

To evaluate how Poisson noise in PNR affects the reflection, we reconstructed the reflection R^- using solely spin-down data (Figure A.1), in comparison to R^+ (Figure 4a). The expected reflection (obtained by fitting) and reconstructed reflection is depicted in Figure A.2. The errors of R^- for $q \geq 0.08 \text{ \AA}^{-1}$ encompass nearly the whole range of reflection values and clearly exceed the errors of R^+ . This observation can be explained by the fact that the spin-down reflectivity decays faster (compared to the spin-up reflectivity) and that the measurement uncertainty originating from the background is more pronounced. Comparing, however, the spin-up with the spin-down reflection, both coincide with the true reflection equally well, if averaged over the entire measured q -range.

The reconstruction for q close to the total reflection edge is highly sensitive to noise in the reflectivity, see Figure 4a and Figure A.2 in the range $q \in [0.02, 0.03] \text{ \AA}^{-1}$. The reflection is transformed by equation 3 which has a pole at $|R(q)|^2 = 1$, i.e. at the total reflection edge. Hence, the reconstruction is strongly influenced by noise in the reflectivity data close to the total reflection edge.

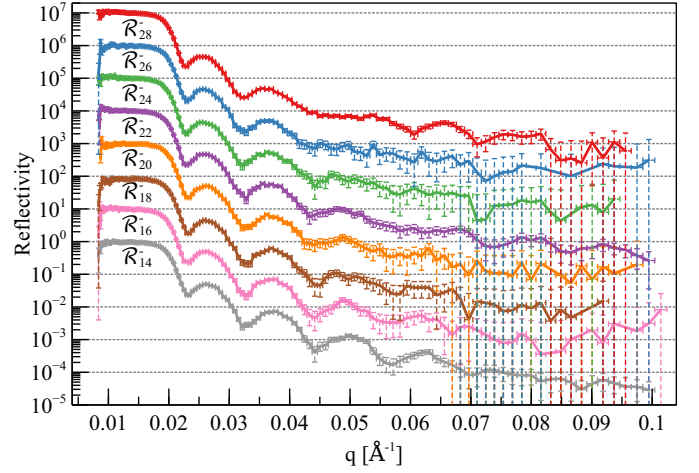


Figure A.1: Neutron reflectivity data \mathcal{R}_n^- of the Si/Cu/Fe sample. Each reflectivity is shifted by one order of magnitude for reasons of clarity. The reflectivity \mathcal{R}_n^- corresponds to the sample with n monolayers of Fe. The sample is magnetized anti-parallel to the neutron spin polarization (spin-down).

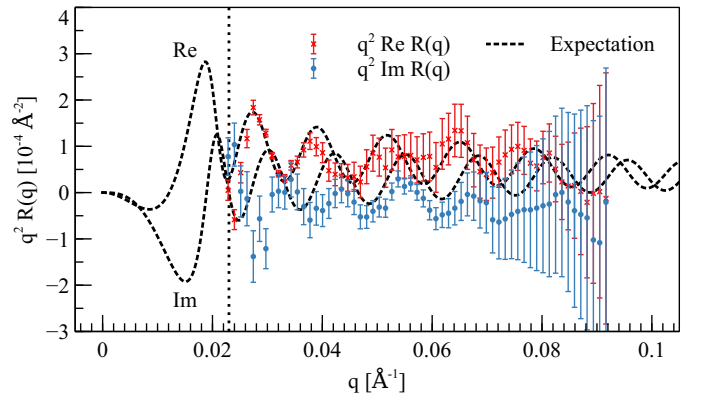


Figure A.2: Reconstructed reflection multiplied with q^2 of the unknown Cu layer, including a remnant Fe layer magnetized anti-parallel to the neutron polarization. The reflection is reconstructed using only the reflectivity data (spin-down) $\mathcal{R}_{16}^- - \mathcal{R}_{28}^-$. The expected reflection represents the sample as in Figure 4a except being magnetized in opposite direction.

Appendix B. Additional Data

The optimal parameters for the reflection model in Section 4.3 are listed for completeness in Table B.1. Only the parameters with a given unit are physically interpreted. The parameter d represents the thickness of the Cu layer, σ is the rms roughness of the Si/Cu interface, ρ is the SLD of Cu, ρ_Δ is the difference in the SLD of Cu and Si, and q_c corresponds to the critical wave vector. The values listed in the column “Expectation” are obtained from a traditional fit of the reflectivity.

Table B.1: Fitted parameters obtained from the reflection model (4) with $\chi_{\text{red}}^2 = 1.38$.

Symbol	Fit	Expectation	Unit
d	433 ± 2	433	\AA
σ	12.2 ± 0.4	10.7	\AA
ρ	5.82 ± 0.04	6.45	10^{-6}\AA^{-2}
ρ_Δ	3.94 ± 0.28	4.38	10^{-6}\AA^{-2}
q_c	0.019 ± 0.001	0.018	\AA^{-1}
a_0	$(1.5 \pm 0.4) \times 10^{-7}$	-	-
a_1	$(7.8 \pm 0.2) \times 10^{-6}$	-	-
ϕ_0	$(0.12 \pm 0.03) \pi$	0	-
ϕ_1	$(-9.3 \pm 0.2) \times 10^{-2}$	-	-

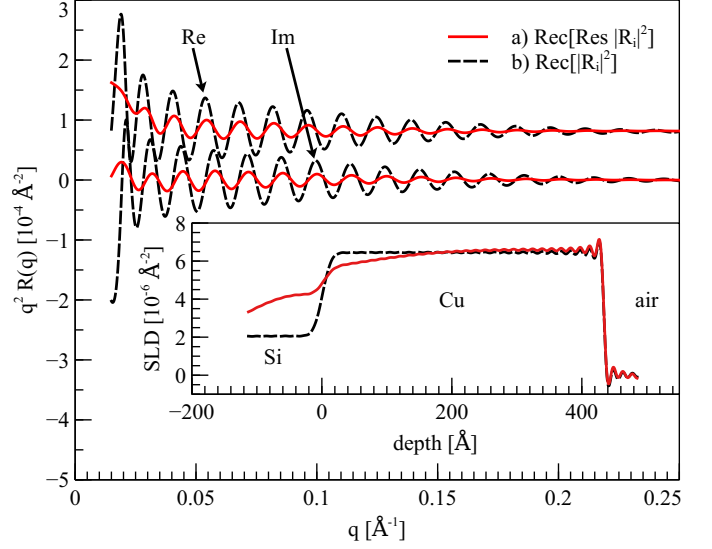


Figure C.3: Simulation of the influence of resolution in reflectivity measurements onto the reconstructed reflection. a) Shows the reconstructed reflection multiplied with q^2 obtained by resolution degraded reflectivity measurements. b) Shows the reconstruction without any degradation. The inset graph depicts the inverted potential of the reflections for $q \in [0, 0.43] \text{\AA}^{-1}$. The true potential is that of a Si substrate with a $\approx 433 \text{\AA}$ thick Cu layer on top.

Appendix C. Resolution Effects

For evaluating the effect of resolution on the reconstructed reflection, we simulated the reflectivity first without including any resolution and then with a constant relative wavelength and constant relative angular resolution. The resolution is given by

$$\Delta q = q \sqrt{\left(\frac{\Delta \lambda}{\lambda}\right)^2 + \left(\frac{\Delta \theta}{\tan(\theta)}\right)^2}.$$

The resolution of the reflectivity $\text{Res } |R|^2$ is computed by the convolution (denoted by $*$) with a normal distribution $\mathcal{N}_{\Delta q}$ with mean $\mu = 0$ and standard deviation $\sigma = \Delta q(q)$ by

$$\text{Res } [|R|^2](q) = (|R|^2 * \mathcal{N}_{\Delta q})(q).$$

The reflection is reconstructed as in Section 4.2, however, using the simulated reflectivity data with and without applied resolution. Taking a constant $\Delta\theta_{\text{FWHM}} \equiv 0.3^\circ$ and $\Delta\lambda_{\text{FWHM}} \equiv 0.2 \text{\AA}$ the reflection together with the corresponding inverted potential is shown in Figure C.3.

In this simple example we observe a damping ($\approx 1 : 3$) of the oscillations and a small phase shift ($\Delta\varphi \approx \pi/13$ rad) in the reconstructed reflection. The resolution degraded potential exhibits a slightly higher ($\approx 2\%$) SLD at the Cu/Fe interface while at the Si/Cu interface the SLD drops as the relative error increases to 10%. At the Si substrate

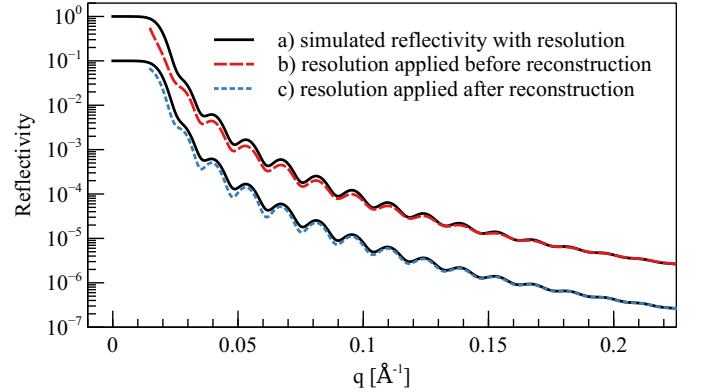


Figure C.4: Computed reflectivities obtained by a) a common reflectivity simulation b) reconstruction of the reflection with resolution degraded reflectivity data c) reconstruction the reflection with perfect reflectivity data and applying the resolution operator afterwards. The reflectivity is shifted by one order of magnitude. Note that a), b) and c) correspond to $\text{Res } |R|^2$, $\text{Rec}[\text{Res}(|R_i|^2)]$ and $\text{Res}^*[\text{Rec}(|R_i|^2)]$, respectively.

the SLD has a mismatch of $> 100\%$, however the thickness of the Cu layer can clearly be identified.

Another interesting observation can be seen in Figure C.4. It shows that the reconstruction operator Rec and the resolution operator Res cannot be interchanged, i.e. none of the following reflections are equal:

$$\text{Rec}[\text{Res}(|R_i|^2)], \quad \text{Res}^*[\text{Rec}(|R_i|^2)], \quad \text{Res}|R|^2$$

where Rec denotes the operator which reconstructs the reflection based on $i \in \mathbb{N}, i \geq 3$ reflectivity measurements $|R_i|^2$ and known reference layers, $|R|^2$ denotes the reflectivity of the sample. Recall that R corresponds to the reflection of the unknown sample whereas R_i corresponds to the reflection of the unknown sample with a reference layer i . The operator Res^* denotes the naive definition of a resolution operator by convoluting the real and imaginary part separately. Note that the equation $\text{Rec}(|R_i|^2) = R$ does hold. Especially, it is not possible to reconstruct the true reflection of the unknown sample from resolution degraded reflectivity data.

It is not straightforward and as such not yet clear how to best remove the resolution from the reflection data since a precise description of how the resolution of an instrument changes the reflection of the sample is not known. A first approach is to remove the resolution already from the reflectivity, e.g. by deconvolution techniques, and then retrieve the reflection. However, a thorough analysis of this problem is beyond the scope of this work, and will be presented elsewhere.

Appendix D. Error Estimation

Since the error propagation and estimation are highly involved, we estimated the errors by numerical Monte-Carlo simulations. The errors of the reflection (for q larger than the minimal wave vector transfer q_c) are calculated by the covariance matrix of the minima of χ^2 in equation (2). The errors for the low q region ($q \leq q_c$) are estimated as follows: From the reflection $R \pm \sigma_R$ one randomly draws 2000 samples R' , from which the reflection $R'(q \leq q_c)$ is retrieved with a fixed-point algorithm [25]. The error in $R(q \leq q_c)$ is then set as the standard deviation of R' . Likewise, the error in the SLD is the standard deviation of 5000 inverted, randomly drawn reflections.

It is noted that this error calculation of the SLD might not be precise: The error in $R(q \leq q_c)$ is calculated from $R(q \geq q_c)$ and thus the errors are in general no longer independent for each q , contrary to our assumption.

Note that the error calculations performed in this paper do not include possible errors in the parameters of the reference layers (Table 1).

References

- [1] H. Fiedeldey, R. Lipperheide, H. Leeb, S. Sofianos, A proposal for the determination of the phases in specular neutron reflection, *Physics Letters A* 170 (1992) 347–351. doi:10.1016/0375-9601(92)90885-P.
- [2] W. L. Clinton, Phase determination in x-ray and neutron reflectivity using logarithmic dispersion relations, *Physical Review B* 48 (1993) 1–5. doi:10.1103/PhysRevB.48.1.
- [3] M. K. Sanyal, S. K. Sinha, A. Gibaud, K. G. Huang, B. L. Carvalho, M. Rafailovich, J. Sokolov, X. Zhao, W. Zhao, Fourier Reconstruction of Density Profiles of Thin Films Using Anomalous X-Ray Reflectivity, *Europhysics Letters (EPL)* 21 (1993) 691–696. doi:10.1209/0295-5075/21/6/010.
- [4] J. E. Lynn, P. A. Seeger, Resonance effects in neutron scattering lengths of rare-earth nuclides, *Atomic Data and Nuclear Data Tables* 44 (1990) 191–207. doi:10.1016/0092-640X(90)90013-A.
- [5] Y. A. Salamatov, E. A. Kravtsov, Use of gadolinium as a reference layer for neutron reflectometry, *Journal of Surface Investigation. X-ray, Synchrotron and Neutron Techniques* 10 (2016) 1169–1172. doi:10.1134/S1027451016050591.
- [6] E. S. Nikova, Y. A. Salamatov, E. A. Kravtsov, M. V. Makarova, V. V. Proglyado, V. V. Ustinov, V. I. Bodnarchuk, A. V. Nagorny, Experimental Approximation of Reference Layer Method in Resonant Neutron Reflectometry, *Physics of Metals and Metallography* 120 (2019) 838–843. doi:10.1134/S0031918X19090102.
- [7] E. S. Nikova, Y. A. Salamatov, E. A. Kravtsov, V. V. Ustinov, V. I. Bodnarchuk, A. V. Nagorny, Development of Reference Layer Method in Resonant Neutron Reflectometry, *Journal of Surface Investigation: X-ray, Synchrotron and Neutron Techniques* 14 (2020) S161–S164. doi:10.1134/S1027451020070344.
- [8] C. F. Majkrzak, N. F. Berk, Exact determination of the phase in neutron reflectometry, *Physical Review B* 52 (1995) 10827–10830. doi:10.1103/PhysRevB.52.10827.
- [9] V.-O. de Haan, A. A. van Well, S. Adenwalla, G. P. Felcher, Retrieval of phase information in neutron reflectometry, *Physical Review B* 52 (1995) 10831–10833. doi:10.1103/PhysRevB.52.10831.
- [10] B. J. Kirby, P. A. Kienzle, B. B. Maranville, N. F. Berk, J. Krycka, F. Heinrich, C. F. Majkrzak, Phase-sensitive specular neutron reflectometry for imaging the nanometer scale composition depth profile of thin-film materials, *Current Opinion in Colloid & Interface Science* 17 (2012) 44–53. doi:10.1016/j.cocis.2011.11.001.
- [11] C. F. Majkrzak, N. F. Berk, J. A. Dura, S. K. Satija, A. Karim, J. Pedulla, R. D. Deslattes, Phase determination and inversion in specular neutron reflectometry, *Physica B: Condensed Matter* 248 (1998) 338–342. doi:10.1016/S0921-4526(98)00260-9.
- [12] C. F. Majkrzak, N. F. Berk, P. Kienzle, U. Perez-Salas, Progress in the Development of Phase-Sensitive Neutron Reflectometry Methods, *Langmuir* 25 (2009) 4154–4161. doi:10.1021/1a802838t.
- [13] C. F. Majkrzak, N. F. Berk, V. Silin, C. W. Meuse, Experimental demonstration of phase determination in neutron reflectometry by variation of the surrounding media, *Physica B: Condensed Matter* 283 (2000) 248–252. doi:10.1016/S0921-4526(99)01985-7.
- [14] H. Leeb, J. Kasper, R. Lipperheide, Determination of the phase in neutron reflectometry by polarization measurements, *Physics Letters A* 239 (1998) 147–152. doi:10.1016/S0375-9601(97)00972-9.
- [15] J. Kasper, H. Leeb, R. Lipperheide, Phase determination in spin-polarized neutron specular reflection, *Phys. Rev. Lett.* 80 (1998) 2614–2617. doi:10.1103/PhysRevLett.80.2614.
- [16] C. F. Majkrzak, N. F. Berk, U. A. Perez-Salas, Phase-Sensitive Neutron Reflectometry, *Langmuir* 19 (2003) 7796–7810. doi:10.1021/1a0341254.
- [17] A. Schmehl, T. Mairoser, A. Herrnberger, C. Stephanos, S. Meir, B. Förg, B. Wiedemann, P. Böni, J. Mannhart, W. Kreuzpaintner, Design and realization of a sputter deposition system for the in situ- and in operando-use in polarized neutron reflectometry experiments, *Nuclear Instruments and Methods in Physics Research Section A: Accelerators, Spectrometers, Detectors and Associated Equipment* 883 (2018) 170–182. doi:10.1016/j.nima.2017.11.086.
- [18] J. Ye, A. Book, S. Mayr, H. Gabold, F. Meng, H. Schäfferer,

- R. Need, D. Gilbert, T. Saerbeck, J. Stahn, P. Böni, W. Kreuzpaintner, Design and realization of a sputter deposition system for the in situ and in operando use in polarized neutron reflectometry experiments: Novel capabilities, *Nuclear Instruments and Methods in Physics Research Section A: Accelerators, Spectrometers, Detectors and Associated Equipment* 964 (2020) 163710. doi:10.1016/j.nima.2020.163710.
- [19] W. Kreuzpaintner, B. Wiedemann, J. Stahn, J.-F. Moulin, S. Mayr, T. Mairoser, A. Schmehl, A. Herrnberger, P. Korelis, M. Haese, J. Ye, M. Pomm, P. Böni, J. Mannhart, *In situ* Polarized Neutron Reflectometry: Epitaxial Thin-Film Growth of Fe on Cu(001) by dc Magnetron Sputtering, *Physical Review Applied* 7 (2017) 054004. doi:10.1103/PhysRevApplied.7.054004.
- [20] J. Stahn, A. Glavic, Focusing neutron reflectometry: Implementation and experience on the TOF-reflectometer Amor, *Nuclear Instruments and Methods in Physics Research Section A: Accelerators, Spectrometers, Detectors and Associated Equipment* 821 (2016) 44–54. doi:10.1016/j.nima.2016.03.007.
- [21] P. E. Sacks, Reconstruction of steplike potentials, *Wave Motion* 18 (1993) 21–30. doi:10.1016/0165-2125(93)90058-N.
- [22] K. Chadan, P. C. Sabatier, *Inverse problems in quantum scattering theory*, Texts and monographs in physics, 2nd ed., rev. and expanded ed., Springer-Verlag, New York, 1989. doi:10.1007/978-3-662-12125-2.
- [23] University of Maryland, DANSE Reflectometry Group, DiRefl (Direct Inversion Reflectometry), (Version 1.1.2) [Computer Software], 2009-. URL: <https://github.com/reflectometry/direfl>.
- [24] A. Book, *DirectInversion (dinv)*, (Version 0.1.0) [Computer Software], 2019. URL: <https://github.com/TUM-E21-ThinFilms/DirectInversion>.
- [25] A. Book, P. A. Kienzle, Retrieval of the complex reflection coefficient below the critical edge for neutron reflectometry, *Physica B: Condensed Matter* 588 (2020) 412181. doi:10.1016/j.physb.2020.412181.
- [26] L. Koester, H. Rauch, E. Seymann, Neutron scattering lengths: A survey of experimental data and methods, *Atomic Data and Nuclear Data Tables* 49 (1991) 65–120. doi:10.1016/0092-640X(91)90012-S.
- [27] N. F. Berk, C. F. Majkrzak, Statistical Analysis of Phase-Inversion Neutron Specular Reflectivity, *Langmuir* 25 (2009) 4132–4144. doi:10.1021/1a802779r.
- [28] E. Hewitt, R. E. Hewitt, The Gibbs-Wilbraham phenomenon: An episode in fourier analysis, *Archive for History of Exact Sciences* 21 (1979) 129–160. doi:10.1007/BF00330404.
- [29] T. P. A. Hase, M. S. Brewer, U. B. Arnalds, M. Ahlberg, V. Kapaklis, M. Björck, L. Bouchenoire, P. Thompson, D. Haskel, Y. Choi, J. Lang, C. Sánchez-Hanke, B. Hjörvarsson, Proximity effects on dimensionality and magnetic ordering in pd/fe/pd trilayers, *Physical Review B* 90 (2014) 104403. doi:10.1103/PhysRevB.90.104403.
- [30] S. Mayr, J. Ye, J. Stahn, B. Knoblich, O. Klein, D. A. Gilbert, M. Albrecht, A. Paul, P. Böni, W. Kreuzpaintner, Indications for dzyaloshinskii-moriya interaction at the pd/fe interface studied by in situ polarized neutron reflectometry, *Physical Review B* 101 (2020) 024404. doi:10.1103/PhysRevB.101.024404.
- [31] S. Ikeda, K. Miura, H. Yamamoto, K. Mizunuma, H. D. Gan, M. Endo, S. Kanai, J. Hayakawa, F. Matsukura, H. Ohno, A perpendicular-anisotropy CoFeB–MgO magnetic tunnel junction, *Nature Materials* 9 (2010) 721–724. doi:10.1038/nmat2804.
- [32] C.-H. Lambert, A. Rajanikanth, T. Hauet, S. Mangin, E. E. Fullerton, S. Andrieu, Quantifying perpendicular magnetic anisotropy at the fe-MgO(001) interface, *Applied Physics Letters* 102 (2013) 122410. doi:10.1063/1.4798291.
- [33] S. A. Montoya, S. Couture, J. J. Chess, J. C. T. Lee, N. Kent, D. Henze, S. K. Sinha, M.-Y. Im, S. D. Kevan, P. Fischer, B. J. McMorrán, V. Lomakin, S. Roy, E. E. Fullerton, Tailoring magnetic energies to form dipole skyrmions and skyrmion lattices, *Physical Review B* 95 (2017) 024415. doi:10.1103/PhysRevB.95.024415.
- [34] S. Woo, K. Litzius, B. Krüger, M.-Y. Im, L. Caretta, K. Richter, M. Mann, A. Krone, R. M. Reeve, M. Weigand, P. Agrawal, I. Lemesh, M.-A. Mawass, P. Fischer, M. Kläui, G. S. D. Beach, Observation of room-temperature magnetic skyrmions and their current-driven dynamics in ultrathin metallic ferromagnets, *Nature Materials* 15 (2016) 501–506. doi:10.1038/nmat4593.
- [35] I. Kozhevnikov, L. Peverini, E. Ziegler, Exact determination of the phase in timeresolved x-ray reflectometry, *Optics Express* 16 (2008) 144. doi:10.1364/OE.16.000144.
- [36] I. Kozhevnikov, L. Peverini, E. Ziegler, Exact solution of the phase problem in in situ x-ray reflectometry of a growing layered film, *Journal of Applied Physics* 104 (2008) 054914. doi:10.1063/1.2968218.